Skyrmion flow in periodically modulated channels

Klaus Raab[1,‡], Maurice Schmitt[1,‡], Maarten A. Brems[1], Jan Rothörl[1], Fabian Kammerbauer[1], Sachin Krishnia[1], Mathias Kläui[1, a)], Peter Virnau[1, b)]

[1] Institut für Physik, Johannes Gutenberg-Universität Mainz, Staudingerweg 7, 55128 Mainz, Germany

‡ These authors contributed equally to the study.

E-mail addresses (Corresponding authors) a) klaeui@uni-mainz.de, b) virnau@uni-mainz.de

Abstract

Magnetic skyrmions, topologically stabilized chiral magnetic textures with particle-like properties have so far primarily been studied statically. Here, we experimentally investigate the dynamics of skyrmion ensembles in metallic thin film conduits where they behave as quasi-particle fluids. By exploiting our access to the full trajectories of all fluid particles by means of time-resolved magneto-optical Kerr microscopy, we demonstrate that boundary conditions of skyrmion fluids can be tuned by modulation of the channel geometry. We observe as a function of channel width deviations from classical flow profiles even into the no- or partial-slip regime. Unlike conventional colloids, the skyrmion Hall effect can also introduce transversal flow-asymmetries and even local motion of single skyrmions against the driving force which we explore with particle-based simulations, demonstrating the unique properties of skyrmion liquid flow that uniquely deviates from previously known behavior of other quasi-particles.

Introduction - Skyrmions are chiral magnetic quasiparticles[1–6] that have attracted significant attention since their discovery[6] in the fields of magnetism and spintronics owing to their topologically enhanced stability[7–9]. Once nucleated, these non-trivial spin textures can be manipulated and moved by using low-power spin-orbit torques induced by electric current[10–13]. These properties make them interesting for potential application in spintronics[1,4,14–25] but also as a model system in statistical physics, as they can be considered a highly tunable, virtually ideal two-dimensional system[26]. Dynamic features like size-control[15,27], stochastic Brownian motion[15,28–30] and skyrmion-skyrmion-[31–33], as well as skyrmion-boundary[31–35] repulsion in patterned structures grant them high experimental value to model rheological 2D phenomena like lattice ordering[6,34], phase transitions[34,36,37] and fluid motion[38,39]. In this context, skyrmion flow is the semi-synchronous, driven motion of individual skyrmions in a dense state[39], confined by other skyrmions into a low density lattice.

Classical incompressible Newtonian fluids in laminar flow obeying the Navier-Stokes equation exhibit Poiseuille flow[40] for which the velocity flow profile along the cross-section of a simple confining geometry with flat walls is parabolic. In the context of Newtonian fluids in laminar flow, the frictional interaction between fluid particles and the wall of the channel leads to the observation of the lowest velocity at the channel's walls, with the highest particle velocity occurring in the middle of the channel. The fulfilment of the no-slip boundary conditions occurs as the velocity of fluid particles at the channel’s wall approaches zero. In cases where the velocity decreases toward the boundaries but does not reach zero, the system satisfies partial-slip conditions[41].

The flow of magnetic skyrmions induced by spin-orbit torques exhibits fluid-like characteristics analogous to, e.g., colloidal fluids[42]. Similar to the latter, skyrmions also move in a rough energy landscape originating from defects in magnetic thin films, so-called pinning sites[43]. In a hypothetical perfect, pinning-free skyrmion sample with straight walls and without stray fields, no interactions exist that slow down skyrmions near the boundary of the system and thus leads to slip boundary conditions. No-slip boundary conditions can be fulfilled artificially in experiments if channels with rough confining walls are used, e.g., by triangular modulation of edges. Notably, this means that the boundary conditions of skyrmion fluids can be controlled by the artificial roughness of the structure edge. Comparable rough geometries have been used to tune the flow in simulations of colloidal systems[44,45]. As the constituent particles of a skyrmion fluid can also be tracked individually in space and time, this makes skyrmion fluids compelling systems to study flow phenomena in two dimensions. Skyrmion flow, the role of confinement, and its application have been reported in work based on simulations[46–49], primarily with a focus on the skyrmion Hall effect[12,50–52]. However, in contrast to colloids, so far little has been studied experimentally about the flow properties of skyrmions.

In this study, we investigate rheological characteristics and dynamics of skyrmion systems and their viability as a dynamical 2D model system. We determine the influence of boundary conditions on skyrmion channel flow experimentally and observe drastically varying velocity profiles. With quasi-particle simulations we explore conditions beyond the current capability of our experimental setup and demonstrate asymmetric channel flow inaccessible to conventional colloidal systems showing how additional complexities of skyrmion dynamics result from the skyrmions’ topological spin structure.

***Experimental skyrmion velocity flow profiles* –** We employ experimental measurements on a thin film sample deposited by magnetron sputtering with the following layers beginning with the seed layer on a thermally oxidized Si substrate: Ta(5)/$Co_{20}Fe_{60}B_{20}$(0.95)/Ta(0.09)/MgO(2)/Ta(5) (respective thicknesses in nanometers in parentheses and relative stoichiometric concentration in percentage). More information on manufacturing of the sample is given in Appendix A. We record the skyrmion dynamics at around 315 K using magneto-optical Kerr effect (MOKE)[53] microscopy with differential imaging technique at a frame rate of 16 frames per second. More information on the experimental protocol is given in Appendix B. Spin-orbit torques induced by electrical currents at the Ta/CoFeB interface cause controllable skyrmion motion[12,54] along the current flow with skyrmion velocities in the μm/s regime at low electric current densities of the order of $10^7 \frac{A}{m^2}$ [16]. The samples' skyrmion-edge and skyrmion-skyrmion repulsion confine the particles in the available space, causing a relatively dense skyrmion state when nucleated[15,33,34] (see Fig. 1. a)). To examine the impact of the imposed boundary conditions on the fluid-like behavior of skyrmions, we have fabricated channels with varying confinements. The confinements include straight and thus sharp (Fig. 1 (a)) wire edges, and diametrically zigzag modulated and thus rough edges (Fig. 1 (c, e)).

To understand the type of flow, we first determine the velocity flow profile of skyrmions from trajectories based on frame-to-frame displacements. Fig. 1 a) shows one frame with tracked skyrmions encircled in red, while Fig. 1 b) displays the resulting experimental velocity flow profile for an applied current density of $5.7 \cdot 10^7 \frac{A}{m^2}$ along the width of the wire. In a straight wire, the velocities exhibit a flow that is not very significantly influenced by the edge of the geometrical confinement. Hence, this setup corresponds to slip conditions. Discrepancies observed between experimental flow and a completely homogeneous skyrmion velocity profile likely arise from pinning effects as discussed in Supplementary Figure 1 [64]. Conversely, the skyrmion velocity profile in the modulated channel with an inner width of 80 μm (see Fig. 1 d)) clearly shows the influence of the modulation: While velocities in the inner part are almost constant, velocities in the outer parts within the triangular modulation rapidly decrease towards the edge, as the skyrmion motion is strongly hindered due to edge repulsion and lower current density. Thus, we can effectively impose partial-slip condition with these boundary modulations.

When we decrease the width of the channel but keep the edge modulation, the flattened region in the center of the velocity profiles can be minimized, or even avoided, as seen in Fig. 1 e and f). In this experiment, the distance between opposing triangle edges is halved to a 40 μm channel width, while the current density stays the same, resulting in an almost parabolic velocity profile, resembling that of a classical fluid. Note, however, that this is a finite-size effect and only occurs in narrow channels while the repulsive interactions stay unaltered.

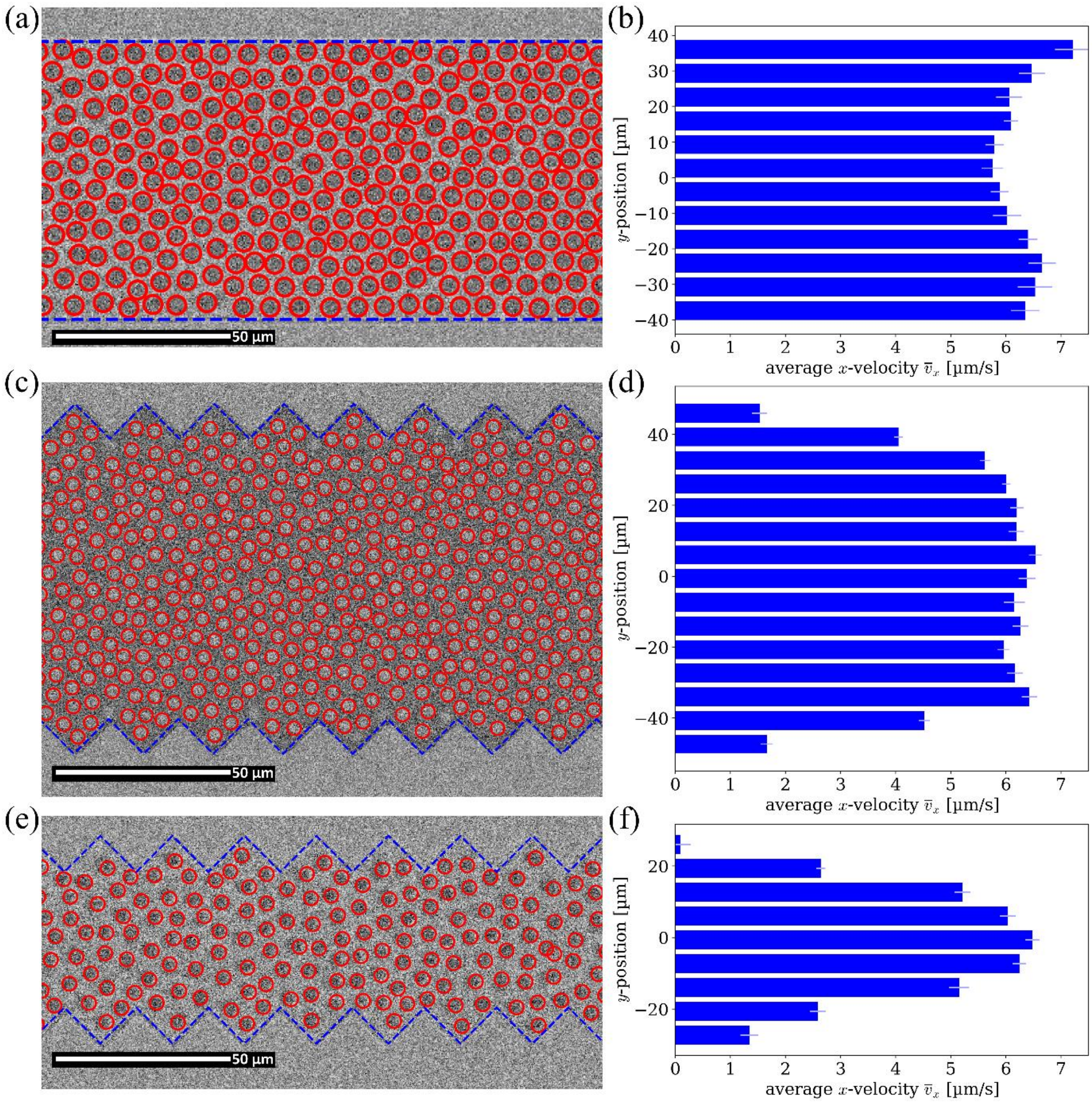

Figure 1: a), c) and e) Single experimental Kerr microscopy frame with skyrmions encircled in red in channels with straight (a) and modulated edges (c, e). Skyrmions are tracked frame by frame and their trajectories are used to extract their respective velocity profiles in x-direction (along the wire). The blue dashed lines help illustrate the channels edge/confinement, which is not visible due to difference imaging. b), d), f) Corresponding velocity profiles; showing the average velocity in µm/s of tracked skyrmions across the channel width (y-axis). Lines at the tip of each histogram bar represent error bars.

To rationalize and better understand the observed behavior, we perform particle-based simulations parametrized to reproduce experimental conditions in the creep regime leading to Fig.1c) and d). Experimental data of rectangular current pulses leads to effective skyrmion Hall angles of $\theta_{skHA} = (0.58 \pm 0.13)°$ [55] and hence corresponding simulations can assume $\theta_{skHA} = 0$ for the presented current densities and corresponding velocities in the creep regime. Note that experimentally, a skyrmion Hall angle of exactly zero is difficult to achieve in the evaluation due to the alignment of the sample and electrical contacts. In a second step, we explore scenarios beyond the capabilities of our current experimental setup and investigate skyrmions with spin structures that go beyond our experimentally realized spin structures leading to strong flow asymmetries arising from non-zero skyrmion Hall angles.

Thiele Model Simulations – Quasi-particle simulations are based on the common form of the Thiele framework[51,56–58] with isotropic dissipation, which is used to describe skyrmions as quasi-particles:[59,60]

$$-\gamma\vec{v} - G^z \times \vec{v} + \vec{F} = 0$$

with friction coefficient γ, instantaneous velocity $\vec{v}$ induced by the total force $\vec{F}$, and gyrotropic vector $G^z = (0,0,G)$ responsible for the skyrmion Hall effect[a]. The corresponding term is set to zero for our first set of simulations while our study of flow asymmetries requires a finite Magnus force. Contributions to the total force $\vec{F}$ are a driving force $\vec{F}_D$, replicating spin-orbit torque induced motion through a confining geometry, a random force $\vec{F}_R$ to mimic Brownian diffusive motion observed in skyrmions, as well as purely repulsive skyrmion-skyrmion and skyrmion-boundary interactions based on previous results of iterative Boltzmann inversion[33]. Note that conventional colloidal systems are also simulated with a similar overdamped Langevin equation which, however, typically does not contain a gyro tropic term required to induce flow asymmetries[61,62] and thus skyrmion flow dynamics exhibits additional complexity not found in conventional colloids. Further details on the simulation protocol and chosen parameters are given in Appendix C of the Supplementary Material[64]. As there is no inertia in the model, skyrmions in the middle of the confining geometry approximately flow with velocity $|\vec{v}_{max}|$ directly induced by the driving force $\vec{F}_D$ in the center:

$$|\vec{v}| = |\vec{v}_{max}| = \frac{|\vec{F}_D|}{\gamma} .$$

The applied driving forces directly follow current density distributions corresponding to each experimental sample, which are obtained using the COMSOL software package[63]. One exemplary current distribution of a sample with modulated edges is given in Supplementary Figure 2 [64].

Simulations of symmetric channel flow – First, simulations with a negligible skyrmion Hall effect (γ = 1, G = 0) were performed and reproduce the creep regime behavior observed in Fig. 1c), d). The average velocity only decreases in the immediate vicinity of the modulation, while skyrmions in the

---

[a] It is important to ensure that the dissipative force opposes the total force, whereas the sign of the Magnus force does not affect the results except for a spatial reflection. In some of our previous publications[32,33,35] there have been typos concerning the sign of the dissipative force. All simulations have however been using the correct equations.

inner part of the channel flow almost homogeneously as they are accelerated back to $|\vec{v}_{max}|$ immediately after collisions due to lack of inertia. The resulting flat profile in the center of the channel (Fig. 2 red) is in good agreement with corresponding experimental results (Fig. 2 blue) confirming the viability of our approach. In comparison, skyrmion flow in a straight channel without modulation (not shown here) is not significantly hindered and the velocity profile is flat even close to the confining boundaries. We conclude that the flow behavior does not resemble that of a classical fluid but is indeed very similar to behavior expected for other quasi-particle systems such as colloids as both can be modelled using similar equations of motion. See Appendix C of the Supplementary Material for further information on simulation parameters[64].

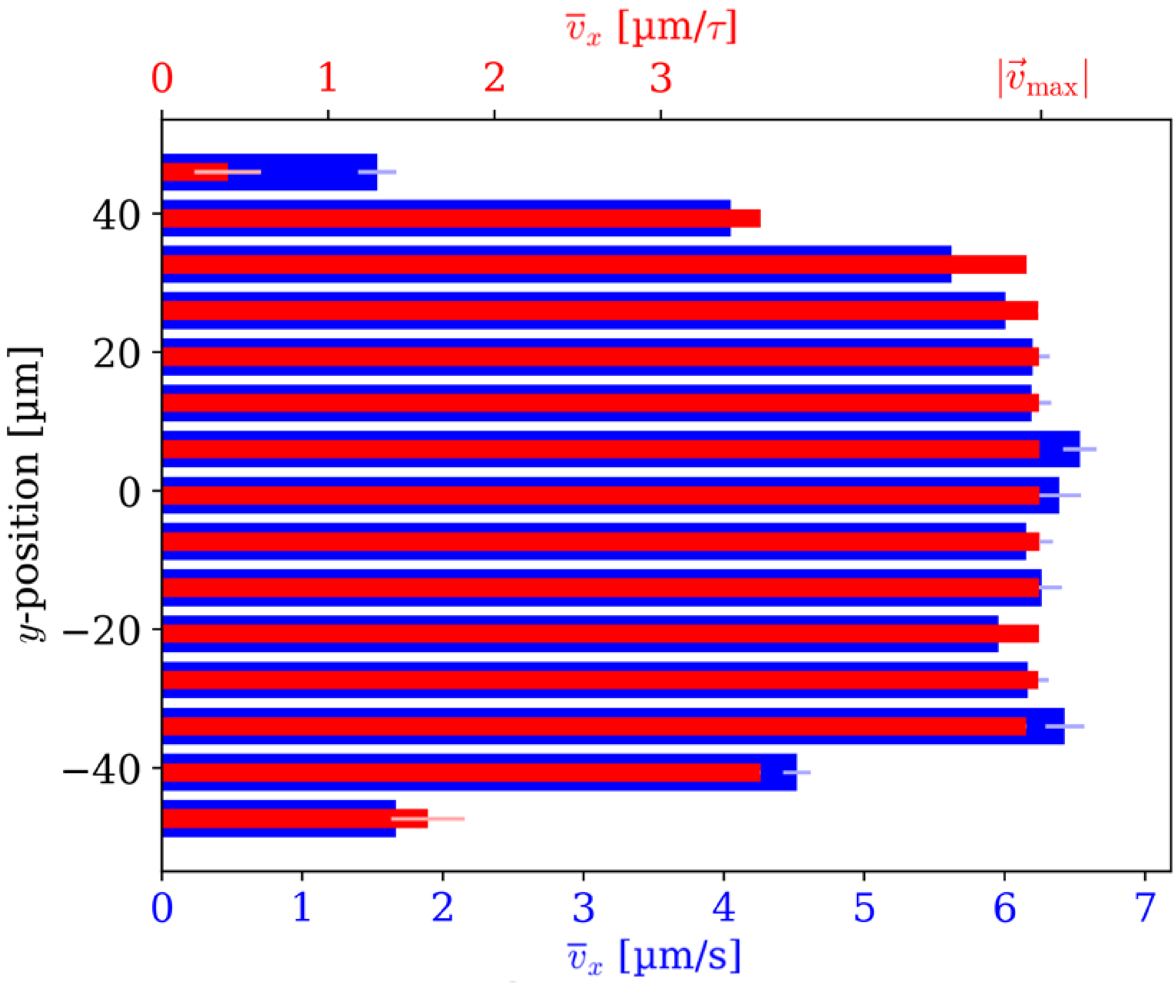

Figure 2: Skyrmion flow velocity profiles of the modulated channel of 80 µm width. Comparison of averaged experimental (blue, in µm/s) and simulated (red, in µm/τ with τ the simulation time parameter) velocity profiles. Both profiles become flat in the inner part of the channel.

Simulations of asymmetric channel flow and local backflow – While so far, our simulations did not consider the Magnus term, in the next step we include this term to account for the skyrmion Hall effect. With non-zero skyrmion Hall angles, the mirror symmetry of the velocity flow profiles with respect to the center of the channel is broken and driving forces push skyrmions preferentially to one side of the sample. This does not only lead to asymmetric skyrmion flow, but reinforced interactions with the boundaries of the confining geometry enabling interesting and more complex flow phenomena inaccessible to conventional colloidal systems. One of these examples we discuss below. At a particular driving force, the average velocity of skyrmions flowing near the top edge of the geometry becomes negative in simulations with a Magnus parameter of G = 0.25, resulting in a skyrmion Hall angle of $\theta_{skHA} = 15°$, i.e., skyrmions propagate opposite to the applied force. The striking asymmetry in the simulated velocity flow profile between the upper half of the confining geometry and the lower half is shown in Fig. 3a). Notably, the velocity increases significantly towards the lower edge, while the velocity towards the upper edge decreases and even becomes negative. These asymmetries are purely caused by the skyrmion Hall effect, since all forces and the confinement are symmetric in our simulations and there are no pinning-effects in this system. Similar asymmetries might be observable in experiments with larger applied current densities where the skyrmion Hall effect is not suppressed[55] and the effects of pinning are overcome. However, tracking the dynamics of skyrmions within the viscous flow regime (velocities on the order of m/s)[55] while a direct current is applied is currently not possible in our experimental setup. The negative velocity at the top edge of the confining geometry in these simulations is caused by a dynamic effect in which one skyrmion forces another one towards the upper boundary of the confining geometry, which then moves against the flow direction along the contour of the modulation. As sketched in Fig. 3b), a skyrmion (marked in red) can be shoved into the space between two modulating triangles by a skyrmion located directly behind it (marked in blue). Notably, this only occurs frequently at the top edge of the confining geometry since skyrmions are constantly pushed downwards by the skyrmion Hall effect, thus leaving more room for a skyrmion to be pushed towards the upper edge of the confining geometry. After following the contour of the modulation, the skyrmion marked as red realigns with the flowing skyrmions in the bulk, effectively switching positions with the skyrmion marked as blue. During this process, the red skyrmion is pushed against the direction of applied current, which is significantly lower in between the triangular modulation (see Suppl. Fig. 2), thus resulting in a negative velocity for that particular bin. Note, however, that this effect does not lead to an effective backflow as skyrmions are propelled in the flow direction as soon as they move away from the upper confining boundary. This backflow effect occurs for various geometries, and it is particularly pronounced in the geometry shown in Fig. 3. It can also occur when the confining geometry has no modulation, i.e., is completely flat; the balance of the driving force and skyrmion Hall angle can create a sufficiently low particle density near the upper confining boundaries such that skyrmions can be pushed closer towards the upper boundaries and exhibit this demonstrated backflow effect. Further geometries exhibiting backflow are shown in appendix D of the Supplementary Materials[64].

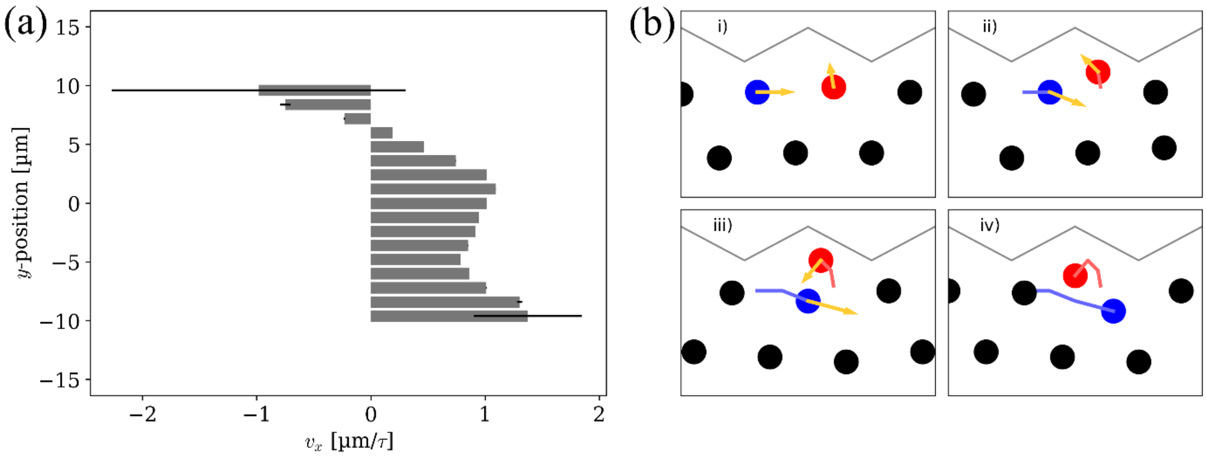

Figure 3: a) Simulated velocity flow profile of a 20 µm channel with oblate modulation (see b)) and a skyrmion Hall angle set to $\theta_{skHA} = 15°$, resulting in an asymmetric velocity flow profile. Notably, the average skyrmion velocity at the upper edge of the confining geometry is negative, implying that skyrmions in this region flow opposite to the applied driving force. b) Sketch of a dynamic process which occurs at the upper edge of the confining geometry, leading to negative velocities on average. Skyrmions experiencing a force from left to right will also be pushed downwards due to the skyrmion Hall effect. As a result, a skyrmion (marked red) can be pushed into the space created between the flowing skyrmions and two triangle tips (i-ii). (iii-iv) Then the red skyrmion slightly moves against the applied current and finally moves back in line with the flowing skyrmions, behind the skyrmion it was initially ahead of.

***Conclusion* -** In this paper, we determine the characteristics of skyrmion quasi-particle flow in a low velocity, current driven creep regime in two-dimensional channels by combining experiments and simulations. We demonstrate that a large variety of flow profiles can be obtained by tuning the confining boundaries. A regular triangular modulation hinders movement of skyrmions along the boundaries effectively imposing partial-slip conditions, while flat boundaries provide slip conditions. In the modulated case we obtain an almost parabolic flow profile for small channels and driving forces, while velocities flatten in the middle of wider channels. On a fundamental level, skyrmion quasi-particles can thus share many transport characteristics with other macroscopic particles in overdamped scenarios like colloids. While previous studies of skyrmion fluid dynamics have been very limited, the ability to tune the boundary conditions of skyrmion flow in combination with various skyrmion-specific effects grants skyrmion fluids high potential for interdisciplinary research beyond what is possible in conventional systems. For instance, unlike the conventional (quasi-) particles, asymmetries arising from Magnus forces enable a whole new variety of phenomena including local backflow which we demonstrate with particle-based simulations. This together with the ability to adjust sizes and densities of skyrmions on the fly underscores their potential as a highly tunable model system for studying fundamental aspects of forces and transport in statistical physics.

Code availability

The computer codes used for data analysis are available upon reasonable request from the corresponding authors.

Data availability

The data supporting the findings of this work are available from the corresponding authors upon reasonable request.

Acknowledgements

P. V. acknowledges helpful discussions with M. Lukacova. The work was supported by the Deutsche Forschungsgemeinschaft (DFG, German Research Foundation) projects 403502522 (SPP 2137 Skyrmionics), 49741853, and 268565370 (SFB TRR173 projects A01 and B02), TopDyn and ERC-2019-SyG no. 856538 (3D MAGiC). P. V., M. S., M. B. and J. R. acknowledge funding from DFG SFB TRR 146 (project #233630050). M. B. is supported by a doctoral scholarship of the Studienstiftung des deutschen Volkes. The authors gratefully *acknowledge* the computing time granted on the supercomputer MOGON II and III at Johannes Gutenberg University Mainz as part of *NHR* South-West.

Author Contributions

M. K. and P. V. devised and supervised the study. F. K. sputtered the sample. K. R. designed and fabricated the sample and carried out the measurements. K. R. and M. S. tracked and analyzed recorded videos. M. S. performed the simulation and analyzed the flow data with the help of M. B. and J. R.. The manuscript was prepared by M. S., K. R., M. B. and P. V.; all authors commented on the manuscript.

Competing Interests

The authors declare no conflict of interest.

References

1. Fert, A., Reyren, N. & Cros, V. Magnetic skyrmions: advances in physics and potential applications. *Nat. Rev. Mater.* **2**, 17031 (2017).
2. Bogdanov, A. N. & Panagopoulos, C. Physical foundations and basic properties of magnetic skyrmions. *Nat. Rev. Phys.* **2**, 492–498 (2020).
3. Jiang, W. *et al.* Skyrmions in magnetic multilayers. *Phys. Rep.* **704**, 1–49 (2017).
4. Finocchio, G., Büttner, F., Tomasello, R., Carpentieri, M. & Kläui, M. Magnetic skyrmions: from fundamental to applications. *J. Phys. Appl. Phys.* **49**, 423001 (2016).
5. Wiesendanger, R. Nanoscale magnetic skyrmions in metallic films and multilayers: a new twist for spintronics. *Nat. Rev. Mater.* **1**, 16044 (2016).
6. Mühlbauer, S. *et al.* Skyrmion Lattice in a Chiral Magnet. *Science* **323**, 915–919 (2009).
7. Pokrovsky, V. L. Properties of ordered, continuously degenerate systems. *Adv. Phys.* **28**, 595–656 (1979).
8. Bogdanov, A. & Hubert, A. Thermodynamically stable magnetic vortex states in magnetic crystals. *J. Magn. Magn. Mater.* **138**, 255–269 (1994).
9. Je, S.-G. *et al.* Direct Demonstration of Topological Stability of Magnetic Skyrmions via Topology Manipulation. *ACS Nano* **14**, 3251–3258 (2020).
10. Sampaio, J., Cros, V., Rohart, S., Thiaville, A. & Fert, A. Nucleation, stability and current-induced motion of isolated magnetic skyrmions in nanostructures. *Nat. Nanotechnol.* **8**, 839–844 (2013).
11. Jiang, W. *et al.* Blowing magnetic skyrmion bubbles. *Science* **349**, 283–286 (2015).
12. Woo, S. *et al.* Observation of room-temperature magnetic skyrmions and their current-driven dynamics in ultrathin metallic ferromagnets. *Nat. Mater.* **15**, 501–506 (2016).
13. Lemesh, I. *et al.* Current-Induced Skyrmion Generation through Morphological Thermal Transitions in Chiral Ferromagnetic Heterostructures. *Adv. Mater.* **30**, 1805461 (2018).
14. Dohi, T., Reeve, Robert. M. & Kläui, M. Thin Film Skyrmionics. *Annu. Rev. Condens. Matter Phys.* **13**, 73-95 (2022).

15. Zázvorka, J. *et al.* Thermal skyrmion diffusion used in a reshuffler device. *Nat. Nanotechnol.* **14**, 658–661 (2019).
16. Raab, K. *et al.* Brownian reservoir computing realized using geometrically confined skyrmion dynamics. *Nat. Commun.* **13**, 6982 (2022).
17. Prychynenko, D. *et al.* Magnetic Skyrmion as a Nonlinear Resistive Element: A Potential Building Block for Reservoir Computing. *Phys. Rev. Appl.* **9**, 014034 (2018).
18. Pinna, D. *et al.* Skyrmion Gas Manipulation for Probabilistic Computing. *Phys. Rev. Appl.* **9**, 064018 (2018).
19. Jibiki, Y. *et al.* Skyrmion Brownian circuit implemented in continuous ferromagnetic thin film. *Appl. Phys. Lett.* **117**, 082402 (2020).
20. Song, K. M. *et al.* Skyrmion-based artificial synapses for neuromorphic computing. *Nat. Electron.* **3**, 148–155 (2020).
21. Brems, M. A., Kläui, M. & Virnau, P. Circuits and excitations to enable Brownian token-based computing with skyrmions. *Appl. Phys. Lett.* **119**, 132405 (2021).
22. Fert, A., Cros, V. & Sampaio, J. Skyrmions on the track. *Nat. Nanotechnol.* **8**, 152–156 (2013).
23. Li, S. *et al.* Magnetic skyrmions for unconventional computing. *Mater. Horiz.* **8**, 854–868 (2021).
24. Grollier, J., Querlioz, D. & Stiles, M. D. Spintronic Nanodevices for Bioinspired Computing. *Proc. IEEE* **104**, 2024–2039 (2016).
25. Göbel, B. & Mertig, I. Skyrmion ratchet propagation: utilizing the skyrmion Hall effect in AC racetrack storage devices. *Sci. Rep.* **11**, 3020 (2021).
26. Yu, X. Z. *et al.* Real-space observation of a two-dimensional skyrmion crystal. *Nature* **465**, 901–904 (2010).
27. Wang, X. S., Yuan, H. Y. & Wang, X. R. A theory on skyrmion size. *Commun. Phys.* **1**, 31 (2018).
28. Miltat, J., Rohart, S. & Thiaville, A. Brownian motion of magnetic domain walls and skyrmions, and their diffusion constants. *Phys. Rev. B* **97**, 214426 (2018).

29. Miki, S. *et al.* Brownian Motion of Magnetic Skyrmions in One- and Two-Dimensional Systems. *J. Phys. Soc. Jpn.* **90**, 083601 (2021).

30. Troncoso, R. E. & Núñez, Á. S. Brownian motion of massive skyrmions in magnetic thin films. *Ann. Phys.* **351**, 850–856 (2014).

31. Zhang, X. *et al.* Skyrmion-skyrmion and skyrmion-edge repulsions in skyrmion-based racetrack memory. *Sci. Rep.* **5**, 7643 (2015).

32. Song, C. *et al.* Commensurability between Element Symmetry and the Number of Skyrmions Governing Skyrmion Diffusion in Confined Geometries. *Adv. Funct. Mater.* **31**, 2010739 (2021).

33. Ge, Y. *et al.* Constructing coarse-grained skyrmion potentials from experimental data with Iterative Boltzmann Inversion. *Commun. Phys.* **6**, 30 (2023).

34. Zázvorka, J. *et al.* Skyrmion Lattice Phases in Thin Film Multilayer. *Adv. Funct. Mater.* **30**, 2004037 (2020).

35. Winkler, T. B. *et al.* Coarse-graining collective skyrmion dynamics in confined geometries. *Appl. Phys. Lett.* **124**, 022403 (2024).

36. Kapfer, S. C. & Krauth, W. Two-Dimensional Melting: From Liquid-Hexatic Coexistence to Continuous Transitions. *Phys. Rev. Lett.* **114**, 035702 (2015).

37. Huang, P. *et al.* Melting of a skyrmion lattice to a skyrmion liquid via a hexatic phase. *Nat. Nanotechnol.* **15**, 761–767 (2020).

38. Reichhardt, C., Ray, D. & Reichhardt, C. J. O. Collective Transport Properties of Driven Skyrmions with Random Disorder. *Phys. Rev. Lett.* **114**, 217202 (2015).

39. Zhang, X. *et al.* Laminar and transiently disordered dynamics of magnetic-skyrmion pipe flow. *Phys. Rev. B* **108**, 144428 (2023).

40. Sutera, S. P. & Skalak, R. The History of Poiseuille's Law. *Annu. Rev. Fluid Mech.* **25**, 1–20 (1993).

41. Thompson, P. A. & Troian, S. M. A general boundary condition for liquid flow at solid surfaces. *Nature* **389**, 360–362 (1997).

42. Vermant, J. & Solomon, M. J. Flow-induced structure in colloidal suspensions. *J. Phys. Condens. Matter* **17**, R187–R216 (2005).

43. Gruber, R. *et al.* Skyrmion pinning energetics in thin film systems. *Nat. Commun.* **13**, 3144 (2022).

44. Isa, L., Besseling, R. & Poon, W. C. K. Shear Zones and Wall Slip in the Capillary Flow of Concentrated Colloidal Suspensions. *Phys. Rev. Lett.* **98**, 198305 (2007).

45. Cloitre, M. & Bonnecaze, R. T. A review on wall slip in high solid dispersions. *Rheol. Acta* **56**, 283–305 (2017).

46. Souza, J. C. B., Vizarim, N. P., Reichhardt, C. J. O., Reichhardt, C. & Venegas, P. A. Skyrmion ratchet in funnel geometries. *Phys. Rev. B* **104**, 054434 (2021).

47. Bellizotti Souza, J. C., Vizarim, N. P., Reichhardt, C. J. O., Reichhardt, C. & Venegas, P. A. Magnus induced diode effect for skyrmions in channels with periodic potentials. *J. Phys. Condens. Matter* **35**, 015804 (2023).

48. Stidham, J. & Pleimling, M. Driven magnetic skyrmions in a narrow channel. *Eur. Phys. J. Spec. Top.* **232**, 1835–1842 (2023).

49. Rocha, F. S. *et al.* Skyrmion transport and annihilation in funnel geometries. *J. Phys. Condens. Matter* **36**, 115801 (2024).

50. Reichhardt, C. & Olson Reichhardt, C. J. Noise fluctuations and drive dependence of the skyrmion Hall effect in disordered systems. *New J. Phys.* **18**, 095005 (2016).

51. Brown, B. L., Täuber, U. C. & Pleimling, M. Effect of the Magnus force on skyrmion relaxation dynamics. *Phys. Rev. B* **97**, 020405 (2018).

52. Reichhardt, C. & Reichhardt, C. J. O. Thermal creep and the skyrmion Hall angle in driven skyrmion crystals. *J. Phys. Condens. Matter* **31**, 07LT01 (2019).

53. McCord, J. Progress in magnetic domain observation by advanced magneto-optical microscopy. *J. Phys. Appl. Phys.* **48**, 333001 (2015).

54. Litzius, K. *et al.* Skyrmion Hall effect revealed by direct time-resolved X-ray microscopy. *Nat. Phys.* **13**, 170–175 (2017).

55. Litzius, K. *et al.* The role of temperature and drive current in skyrmion dynamics. *Nat. Electron.* **3**, 30–36 (2020).

56. Thiele, A. A. Steady-State Motion of Magnetic Domains. *Phys. Rev. Lett.* **30**, 230–233 (1973).

57. Reichhardt, C., Ray, D. & Reichhardt, C. J. O. Quantized transport for a skyrmion moving on a two-dimensional periodic substrate. *Phys. Rev. B* **91**, 104426 (2015).

58. Brown, B. L., Täuber, U. C. & Pleimling, M. Skyrmion relaxation dynamics in the presence of quenched disorder. *Phys. Rev. B* **100**, 024410 (2019).

59. Weißenhofer, M., Rózsa, L. & Nowak, U. Skyrmion Dynamics at Finite Temperatures: Beyond Thiele's Equation. *Phys. Rev. Lett.* **127**, 047203 (2021).

60. Abera Kolech, B. Magnetic Skyrmions and Quasi Particles: A Review on Principles and Applications. in *Vortex Simulation and Identification* (IntechOpen, 2023).

61. Chen, J. C. & Kim, A. S. Brownian Dynamics, Molecular Dynamics, and Monte Carlo modeling of colloidal systems. *Adv. Colloid Interface Sci.* **112**, 159–173 (2004).

62. Unni, H. N. & Yang, C. Brownian dynamics simulation and experimental study of colloidal particle deposition in a microchannel flow. *J. Colloid Interface Sci.* **291**, 28–36 (2005).

63. COMSOL Multiphysics. v. 6.0 www.comsol.com. COMSOL AB, Stockholm, Sweden. (2021).

64. See Supplementary Material [link to be inserted by publisher] for Appendices A-D and supplementary figures 1-3, including further information. Appendix A is about the sample fabrication and current-induced skyrmion motion; appendix B is about Kerr microscopy, video recording and analysis techniques; appendix C considers simulation and simulation parameters; appendix D and supplementary figure 3 provide details on local backflow in varying modulation, supplementary figure 1 shows $+\bar{v}_x$ & -$\bar{v}_x$ velocity profiles of the same channel and supplementary figure 2 shows a simulated current density distribution.COMSOL simulated current density distribution.